

Entanglement Properties of Localized States in 1D Topological Quantum Walks

C.M. Chandrashekhar,^{1,*} H. Obuse,^{2,†} and Th. Busch^{1,‡}

¹*Quantum Systems Unit, Okinawa Institute of Science and Technology Graduate University, Okinawa, Japan*

²*Department of Applied Physics, Hokkaido University, Sapporo 060-8628, Japan*

The symmetries associated with discrete-time quantum walks (DTQWs) and the flexibilities in controlling their dynamical parameters are known to allow creating large number of topological phases. An interface in position space, which separates two regions which have different topological numbers associated with them can, for example, be effectively modelled using different coin parameters for the walk on either side of the interface. Depending on the neighbouring numbers, this can lead to localized states in one-dimensional configurations and here we carry out a detailed study into the strength of such localized states and relate it to the amount of entanglement created by the walks. We show that the entanglement is minimised for strong localizations and that this feature also persists in the presence of small amounts of σ_x (bit flip) noise.

I. INTRODUCTION

Quantum walks, proposed as a quantum analogs of classical random walks^{1,2}, can allow to create non-classical states efficiently and have therefore been used to design superior quantum algorithms^{3–9} and to realize universal quantum computation^{10,11}. In recent years, quantum walks have also been employed to understand the dynamics of a considerable range of other physical processes, for example the simulations of an electric-field driven system¹², the transport in biological or chemical systems^{13–15} or the simulations of relativistic quantum dynamics^{2,16–19}. One of the more recent topics of interest is the exploration of topological phases in quantum walks.

The topological properties of materials have been a rich source of interesting physics and have led to new class of materials known as topological insulators (TIs)^{20–22}. However, only a small number of natural materials displaying TI phases are known and therefore interest in realizing and controlling the topological properties in artificial materials has been one of the prime research interest in recent years. The discrete-time quantum walk (DTQW) is such a system and, apart from simulating the topological states possible in time-independent lattice Hamiltonians, also allow to see the coin operations as a degree of freedom, which leads to a much richer system^{23–28}. Progress in the theoretical understanding of these systems is going hand in hand with current advancements in experimental implementations and engineering of quantum walks in various physical systems²⁹. Exploring topological phases using DTQWs has therefore emerged as a promising approach to realizing TIs in artificial materials.

The nontrivial topological phase of TIs are intricately linked to the presence or absence of certain symmetries, namely, time-reversal symmetry, particle-hole symmetry, and chiral symmetry³⁰. For one-dimensional DTQWs with the all three symmetries present (belonging to class BDI), the topological properties have recently been studied using a two split-step²³ and four split-step DTQW²⁷. Due to the 2π periodicity of the quasi-energies, the topo-

logical numbers of a 1D DTQW are defined not only for 0 but also for π quasi-energies, which means that the topological numbers become $\mathbb{Z} \times \mathbb{Z}$ winding numbers²⁷. Consequently, at the interface where two domains with different topological numbers are connected, topologically protected surface states appear at the two specific quasi-energies. Because of the one-dimensionality and the particle-hole symmetry, these surface states are the Majorana edge states, which are localized at the the interface and which have been experimentally observed²⁵.

As the winding number is a function of the angle θ_i used in the quantum coin operation for each split-step, the phase diagram of a TI can be written in terms of the angle on either side of the interface and the ones that lead to the appearance of localized states at the interface can be identified. However, this only allows to identify configurations for which localized states exist, but does not give any information about the strength of the localization, i.e. the probability of finding the particle at the interface. For some configurations the localization is very strong with a very insignificant probability of finding the particle away from the interface, for others it is very weak with a significant probability of finding the particle away from the interface. Knowing which configurations result in strongly topologically localized states is very useful to simulate TIs with a strongly insulating bandstructure.

In the following we will use negativity as a measure of quantum entanglement and show that for both, the two split-step and the four split-step DTQW, a minimum in the entanglement is observed for values of θ_i that result in localized states due to topological effects at the interface. This behavior is in contrast to the behavior of entanglement for localized states due to disordered coin operations in the DTQW evolution. In particular, compared to the entanglement created in the standard DTQW, an enhancement is seen for temporal^{31,32} and spatio-temporal disorder and a small decrease is seen for spatial disorder³¹. We will also discuss the effect of noise on topologically localized states and show that they are robust against σ_x (bit flip) noise.

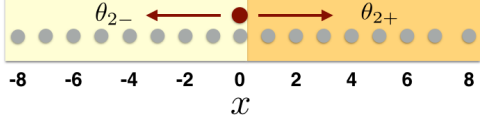


FIG. 1: Schematic of the position space showing the boundary created by θ_{2-} and θ_{2+} , which leads to the appearance of topological properties.

II. TOPOLOGICAL QUANTUM WALKS

A 1D DTQW is defined for a system composed of a particle space and a position space. The basis states of the particle space can be any two internal states represented by $|0\rangle$ and $|1\rangle$ and the basis states of the position space are defined on $|x\rangle$, where x is an integer. If the initial state is given by a particle in state $|\Psi_{\text{in}}\rangle = (\alpha|0\rangle + \beta|1\rangle) \otimes |x=0\rangle$, which is located at the origin, each step of the walk is composed of a quantum coin operation

$$R_\theta \equiv \begin{bmatrix} \cos(\theta/2) & -\sin(\theta/2) \\ \sin(\theta/2) & \cos(\theta/2) \end{bmatrix} \otimes \mathbb{I}, \quad (1)$$

followed by a position shift operation

$$S = |0\rangle\langle 0| \otimes |x-1\rangle\langle x| + |1\rangle\langle 1| \otimes |x+1\rangle\langle x|. \quad (2)$$

The unitary operator $W(\theta) = SR_\theta$ therefore defines one step of the standard DTQW and the state after t steps is given by $|\Psi_t\rangle = [SR_\theta]^t|\Psi_{\text{in}}\rangle$.

The eigenstates of the single time step operator can be written as

$$W(\theta)|\psi_\varepsilon\rangle = e^{-i\varepsilon}|\psi_\varepsilon\rangle, \quad (3)$$

where the quasi-energies ε are real and have 2π periodicity. These spectral properties of $W(\theta)$ give an insight into the long time behavior of the walk, including the topologically protected localized states.

Nontrivial topological phases in DTQW can be found when the evolution operator $W(\theta)$ indicates the presence of certain specific symmetries, such as time-reversal, particle-hole, or chiral symmetries. A nontrivial topological phase in 1D DTQWs requires particle-hole or chiral symmetries to be present²³, which in turn allows the possibility of edge states appearing at $\varepsilon = 0, \pi$. These are localized at the interface where the topological numbers change, which means that the 0 and π quasi-energy states have two different topological quantum numbers ν_0 and ν_π for 0 and π quasi-energy states, respectively²⁷. For the DTQW given above particle-hole symmetry can be assured by realizing that all matrix elements of $W(\theta)$ are real and chiral symmetry is present if $W(\theta)$ satisfies

$$FW(\theta)\Gamma^{-1} = W(\theta)^{-1}, \quad (4)$$

where Γ is the chiral symmetry operator. To confirm the presence of chiral symmetry, we will first decompose the operator $W(\theta)$ into two subsequences F and G

$$W(\theta) = F \cdot G, \quad (5)$$

where F and G are related as

$$\Gamma F F^{-1} = G^{-1}. \quad (6)$$

The above relation is guaranteed if F and G are composed of a coin and shift operators satisfying

$$\Gamma R_\theta \Gamma^{-1} = R_\theta^{-1}, \quad (7)$$

and

$$\Gamma S T^{-1} = S^{-1}, \quad (8)$$

which leads to a chiral symmetry operator of the form

$$\Gamma \equiv \sigma_x \otimes \mathbb{I}, \quad \sigma_x = \begin{bmatrix} 0 & 1 \\ 1 & 0 \end{bmatrix}. \quad (9)$$

The topological numbers (ν_0, ν_π) of the 1D DTQW possessing this kind of chiral symmetry have been calculated recently²⁷. If $W(\theta)$ satisfy chiral symmetry (Eq. (4)), a counterpart state with opposite sign of the quasi-energy is guaranteed,

$$W(\theta)|\psi_{-\varepsilon}\rangle = e^{+i\varepsilon}|\psi_{-\varepsilon}\rangle, \quad (10)$$

where

$$|\psi_{-\varepsilon}\rangle \equiv \Gamma|\psi_\varepsilon\rangle. \quad (11)$$

Taking into account the 2π periodicity of ε , the above relation to the edge states $\varepsilon = 0, \pi$ is identical to the eigenstates of the chiral symmetry operator Γ ,

$$\Gamma|\psi_{0,\pi}\rangle = \pm|\psi_{0,\pi}\rangle, \quad (12)$$

with the eigenvalues ± 1 .

In the following we will focus on the two specific DTQW with chiral symmetry and discuss their topological properties. At first, we consider a DTQW with each step consisting of two split-steps with different coin parameters θ_i ²³,

$$W(\theta_1, \theta_2) = S_+ R_{\theta_2} S_- R_{\theta_1}, \quad (13)$$

and for which the position split shift operators are

$$S_- = |0\rangle\langle 0| \otimes |x-1\rangle\langle x| + |1\rangle\langle 1| \otimes |x\rangle\langle x|; \quad (14)$$

$$S_+ = |0\rangle\langle 0| \otimes |x\rangle\langle x| + |1\rangle\langle 1| \otimes |x+1\rangle\langle x|. \quad (15)$$

To create a real space boundary between the topologically distinct phases and reveal the non-trivial topological properties at the interface, different θ_2 to the left

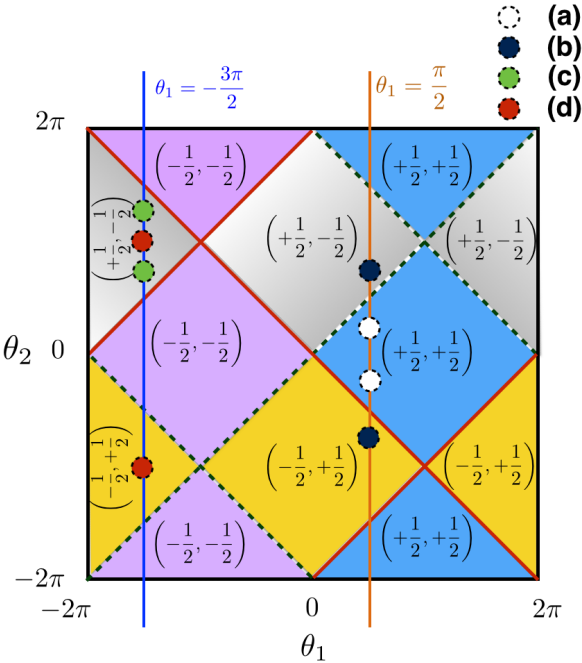


FIG. 2: Phase diagram of the topological numbers (ν_0, ν_π) associated with two split-step DTQW as a function of the coin parameters θ_1 and θ_2 . Topologically distinct gapped phases are separated by lines where the gap closes at either $\varepsilon = 0$ (solid lines) or $\varepsilon = \pi$ (dashed line). Four pairs of circles with different colours and labeled as (a), (b), (c) and (d) are marked to identify different parameters to the left and right side of $x = 0$ used to generate the probability distributions shown in Fig. 3.

$(R_{\theta_{2-}})$ and right side ($R_{\theta_{2+}}$) of the boundary in the position space should be prepared as shown in Fig. 1, while the coin operation R_{θ_1} is defined uniformly on an entire position space.

The topological numbers (ν_0, ν_π) for the two split-step DTQW as a function of the coin parameters θ_1 and θ_2 are shown in Fig. 2²⁶. Using the phase diagram one can identify and choose the regions marked with different colors from which the parameters θ_{2-} and θ_{2+} , to the left side and right side of the position space, respectively are picked.

If θ_{2-} and θ_{2+} are picked from regions with different topological number, the probability of finding the particle at origin ($x = 0$) will remain high, indicating a localized state, whereas if θ_{2+} and θ_{2-} are chosen from a region with the same topological number, the probability at $x = 0$ decrease with time, indicating the absence of a localized state. Examples of this are shown in Fig. 3, where we display the spatial probability distribution after 100 steps for four different configurations of θ_1 , θ_{2+} and θ_{2-} marked in Fig. 2 with circles of identical color. Figs. 3(a) and 3(b) show the cases of $\theta_1 = \pi/2$ and $(\theta_{2+}, \theta_{2-}) = (-\pi/4, \pi/4)$ (same topological invariant) and $(\theta_{2+}, \theta_{2-}) = (-3\pi/4, 3\pi/4)$ (different topological in-

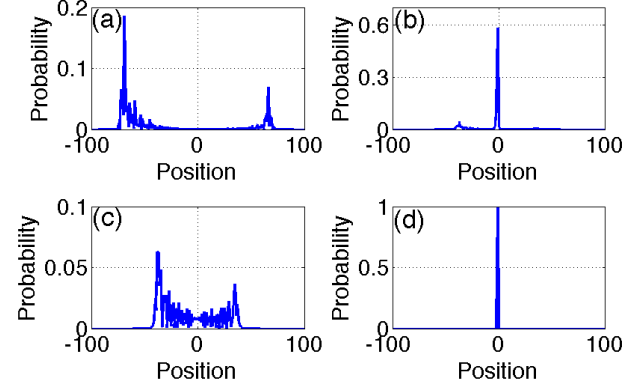


FIG. 3: Probability distributions of the two split-step DTQW after 100 steps with a particle initially in the state $|\Psi_{\text{in}}\rangle = \frac{1}{\sqrt{2}}(|0\rangle + |1\rangle) \otimes |x = 0\rangle$. For (a) and (b) $\theta_1 = \pi/2$ and $(\theta_{2-}, \theta_{2+})$ are $(-\pi/4, \pi/4)$ and $(-3\pi/4, 3\pi/4)$, respectively. For (c) and (d) $\theta_1 = -3\pi/2$ the $(\theta_{2-}, \theta_{2+})$ are $(5\pi/4, 3\pi/4)$ and $(-\pi, \pi)$, respectively. One can see from the circles in Fig. 2 that the parameters chosen for (a) and (c) are in a region with the same topological invariant, resulting in absence of localized state, and parameters for (b) and (d) are in regions with distinct topological numbers, resulting in a localized state.

variant). Similarly, for $\theta_1 = -3\pi/2$ the probability distributions for the combination $(\theta_{2+}, \theta_{2-}) = (5\pi/4, 3\pi/4)$ and $(\theta_{2+}, \theta_{2-}) = (-\pi, \pi)$ are shown in Figs. 3(c) and 3(d). One can clearly see that the probability of being localized at the origin is significant for the combinations with different topological numbers ((b) and (d)), whereas in the other case localization is absent ((a) and (c)).

A second example of a DTQW with rich topological features are the four split-step evolutions²⁷. These are described by four parameters θ_i , leading to an effective Hamiltonian with long range hopping that results in higher values for the winding numbers and the topological numbers. Each four split-step walk is a composition of the operators

$$W(\theta_1, \theta_2, \theta_3, \theta_4) = S_+ R_{\theta_4} S_+ R_{\theta_3} S_- R_{\theta_2} S_- R_{\theta_1}, \quad (16)$$

and setting $\theta_2 = \theta_4$ ensures chiral symmetry (CS). For simplicity we will also set $\theta_1 = 0$ in the following and in Fig. 4 the phase diagram as function of θ_2 and θ_3 is shown. Regions with different topological numbers can be clearly identified²⁷ and in Fig. 5 the spatial probability distributions for the situation in which different coin parameters are used on the left and the right of the initial position, creating a boundary at the interface, are shown. The four pairs of parameters (θ_2, θ_3) used to generate the probability distributions in Fig. 5 are marked with circles of different color in the phase diagram (Fig. 4). For the parameters $(\theta_{2-}, \theta_{2+}; \theta_{3-}, \theta_{3+}) = (-\pi/8, \pi/8; -\pi, \pi)$ and $(-\pi/8, \pi/8; -3\pi/2, -\pi/2)$, chosen from regions with different topological numbers to the left and right side of the origin, the probability of finding the particle at $x = 0$ remains high indicating the presence of

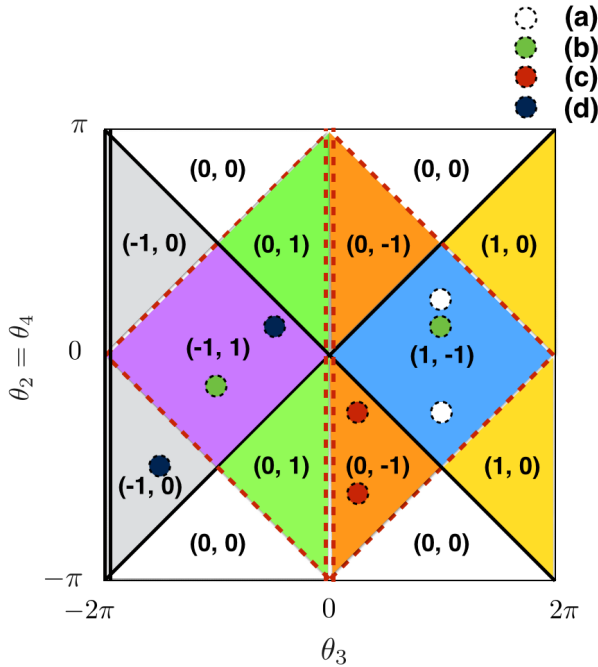


FIG. 4: Phase diagram of the topological numbers associated with four split-step DTQW as a function of the coin parameters θ_2 and θ_3 . The parameters θ_2 and θ_4 are set equal to ensure CS and we have chosen $\theta_1 = 0$. Topologically distinct gapped phases are separated by lines where the gap closes at either $\varepsilon = 0$ (solid lines) or $\varepsilon = \pi$ (dashed line). Four pairs of circles with different shades labeled as (a), (b), (c) and (d) are marked to identify the different parameters to the left and right side of $x = 0$ used to generate probability distributions shown in Fig. 5.

localized state (Figs. 5(b) and 5(d)). For the parameters $(\theta_{2-}, \theta_{2+}; \theta_{3-}, \theta_{3+}) = (-\pi/4, \pi/4; \pi, \pi)$ and $(-\pi/4, 3\pi/4; \pi/4, \pi/4)$, chosen from regions with same topological numbers to the left and right side of the origin, the probability of finding the particle at $x = 0$ is very low indicating the diffusion of the probability of finding the particle at $x = 0$ (Figs. 5(a) and 5(c)). However, we should note that it is possible to generate localized states even for certain sets of parameters from the regions with the same topological invariant. Those localized states have energies different from zero or π and are therefore distinguishable from localized states originating from topological effects.

III. ENTANGLEMENT PROPERTIES OF TOPOLOGICAL QUANTUM WALKS

DTQW are known to entangle the particle and the position space. The degree of entanglement depends on the parameters that define the evolution operators^{33,34} and it is intriguing to explore the degree of entanglement as

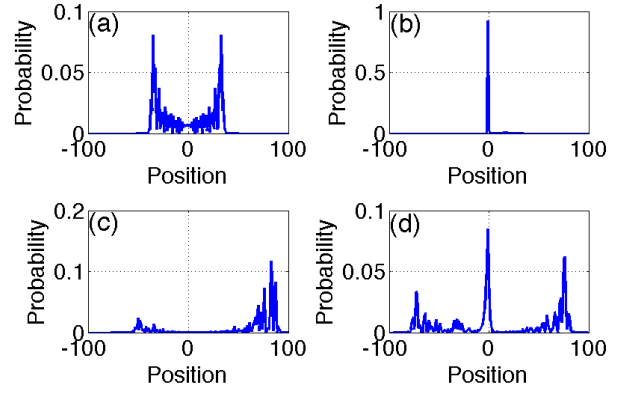


FIG. 5: Probability distributions of the four split-step DTQW after 50 steps of the walk for a particle with the initial state $|\Psi_{\text{in}}\rangle = \frac{1}{\sqrt{2}}(|0\rangle + |1\rangle) \otimes |x = 0\rangle$. The chosen parameters for $(\theta_{2-}, \theta_{2+}; \theta_{3-}, \theta_{3+})$ are marked with circles in Fig. 4, (a) $(-\pi/4, \pi/4; \pi, \pi)$ (b) $(-\pi/8, \pi/8; -\pi, \pi)$, (c) $(-\pi/4, -3\pi/4; \pi/4, \pi/4)$ and (d) $(-\pi/8, \pi/8; -3\pi/2, -\pi/2)$. The parameters in (a) and (c) are from regions with same topological numbers and the absence of a localized state is evident, whereas the parameters in (b) and (d) are from regions with different topological numbers, which leads to localized states.

the function of these parameters for topological quantum walks. In Sec. II we saw that localized states appear when choosing coin parameters for the left and right regions from areas with different topological numbers in the phase diagram. However, this does not guarantee a strongly localized state, which is one with a high probability of finding the particle at $x = 0$. Often the probability of the diffusing component can be higher than the one of the localized part. In this section we ask and answer the question if entanglement is an effective measure to identify the configurations of parameters that result in strongly localized states. Being able to identify parameter regions for walks which simulate strongly topologically localized states is very useful for the artificial synthesis of TIs. We therefore in the following explore the entanglement generated by different topological quantum walks and identify the regions which lead to strongly localized states.

To quantify the entanglement between the particle and the position space we will use negativity, which is the absolute sum of the negative eigenvalues of the partial transpose of $\rho = |\Psi_t\rangle\langle\Psi_t|$

$$\mathcal{N}(\rho) = \sum_i \frac{|\lambda_i| - \lambda_i}{2} \quad (17)$$

where the λ_i are the eigenvalues.

To reduce the number of free parameters we initially fix $\theta_1 = -3\pi/2$ for the two split-step DTQW and show in Fig. 6 the negativity as function of θ_{2-} and θ_{2+} . A varied landscape is clearly visible and to interpret the structure, we can map the diagram to the one for the topological

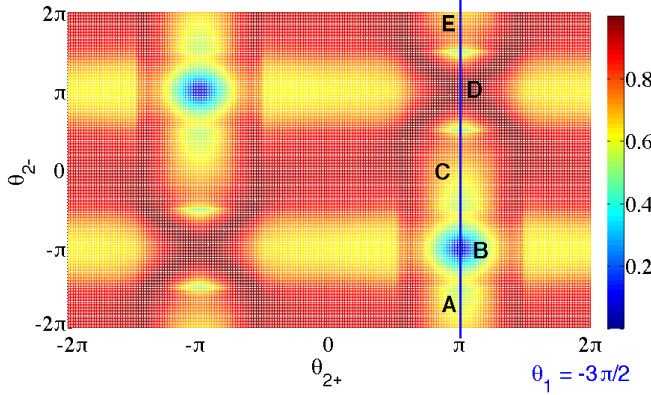


FIG. 6: Negativity as a function of θ_{2-} and θ_{2+} for the two split-step DTQW when θ_1 is fixed at $-3\pi/2$. The initial state was given by $|\Psi_{\text{in}}\rangle = \frac{1}{\sqrt{2}}(|0\rangle + |1\rangle) \otimes |x=0\rangle$ and the results shown are after 100 steps of walk.

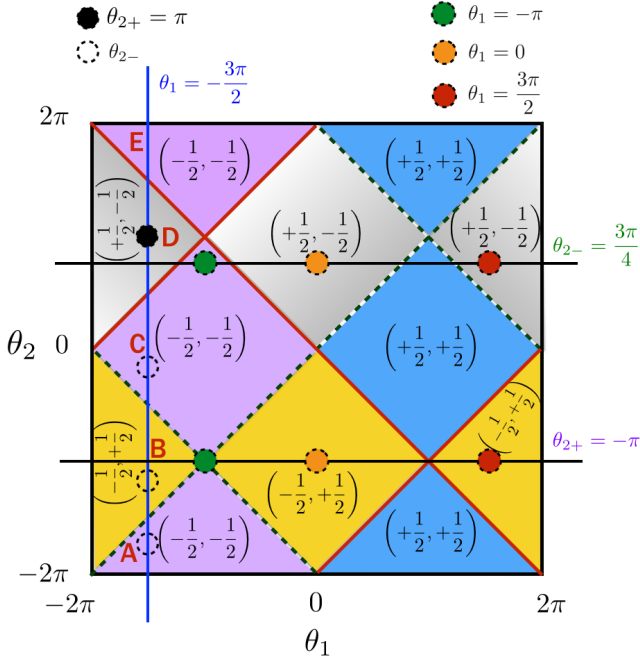


FIG. 7: Phase diagram of a two split-step DTQW identifying the parameters and corresponding topological numbers used for the evolution to obtain the negativity. The vertical line corresponds to the results shown in Fig. 6 and the horizontal lines corresponds to the negativity presented in Fig. 8.

numbers.

For this we show in Fig. 7 the phase diagram again and the vertical line at $\theta_1 = -3\pi/2$ indicates the parameters for which the negativity is displayed in Fig. 6. If $\theta_{2+} = \pi$ (marked with a filled circle in region **D**) and θ_{2-} is spanned from -2π to 2π , one can see that the

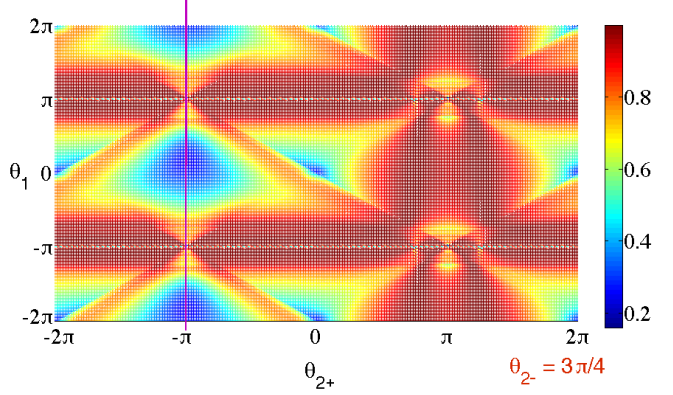


FIG. 8: Negativity of a two split-step DTQW as a function of θ_1 and θ_{2+} when $\theta_{2-} = 3\pi/4$. The initial state was $|\Psi_{\text{in}}\rangle = \frac{1}{\sqrt{2}}(|0\rangle + |1\rangle) \otimes |x=0\rangle$ and the results shown are after 100 steps of walk.

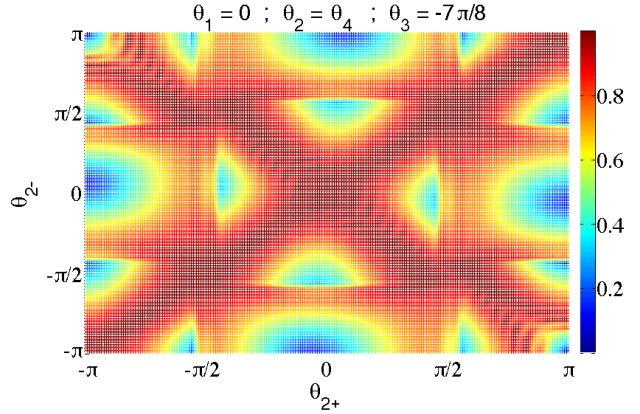


FIG. 9: Negativity of a four split-step DTQW as a function of θ_{2-} and θ_{2+} when $\theta_1 = 0$, $\theta_3 = -7\pi/8$ and $\theta_{4\pm} = \theta_{2\pm}$. The initial state was $|\Psi_{\text{in}}\rangle = \frac{1}{\sqrt{2}}(|0\rangle + |1\rangle) \otimes |x=0\rangle$ and the results shown are after 50 steps of walk.

value of negativity is high when both, θ_{2+} and θ_{2-} , are chosen from a region with the same topological invariant (here **D**). When θ_{2-} is chosen from a region with different topological invariant (**A**, **B**, **C**, or **E**) the values of the negativity are lower and a minimum appears when θ_{2-} is from region **B**. Lower values of negativity indicate the presence of localized state with only a smaller fraction of the particle's amplitude contributing to the diffusion (see Fig. 3(d)).

In Fig. 8 we show the negativity as a function of θ_1 and θ_{2+} by fixing $\theta_{2-} = 3\pi/4$. When $\theta_{2+} = -\pi$ the values of θ_{2-} and θ_{2+} will be in regions with different topological numbers for all values of θ_1 , except for $\theta_1 = \pm\pi$. The pair of horizontal lines in Fig. 7 indicates the regions in which θ_{2-} and θ_{2+} lie when θ_1 is spanned from -2π to 2π and the corresponding values of negativity can

be seen along the vertical line in Fig. 8. One can see that the value of negativity is very low for all values of θ_1 except at the points $\theta_1 = \pm\pi$ where regions of different topological numbers meet. Comparing the phase diagram (Fig. 7) and the negativity profiles (Figs. 6 and 8) for different combinations of θ_1 , θ_{2-} and θ_{2+} one notices that low values for the negativity occur whenever the combination of θ_{2-} and θ_{2+} is chosen from regions with different topological invariant. This indicates that a low area in the negativity landscape can be effectively used to identify the combinations that result in localized states and the minima correspond to localized states with zero or minimal diffusion component.

Similarly, a negativity plot for the four split-step DTQW can be effectively used to identify the combination of parameters which lead to strongly localized states. In Fig. 9 we show the negativity as a function of θ_{2+} and θ_{2-} for $\theta_1 = 0$, $\theta_3 = -7\pi/8$ and $\theta_{4\pm} = \theta_{2\pm}$. The visible valleys of entanglement corresponds to parameter ranges in which a strongly localized state is obtained.

This observation is in contrast to the behavior of entanglement for localization in 1D DTQW using disordered quantum coin operations. With spatially disordered coin operations, only a small decrease in entanglement is seen when compared to the entanglement due to standard DTQW³¹. With temporally and spatio-temporally disordered coin operations, enhancement of entanglement is seen^{31,32}. Though the states are localized, the degree of entanglement is not significantly affected because of the longer localization length of the disordered localized state when compared to the short localization length of topologically localized states.

IV. STRENGTH OF THE LOCALIZED STATE AND THE EFFECT OF NOISE

The application of noise to DTQWs is known to result in decoherence^{33,35}, however small amounts of noise can also be advantageous for quantum algorithms and quantum transport. Here we will look into the effect of $\sigma_x = \begin{bmatrix} 0 & 1 \\ 1 & 0 \end{bmatrix}$ (bit flip) noise on the topological quantum walk, which results in localized states, and compare it to the evolution when the localized state is absent.

The operation used for describing the two split-step DTQW evolution with σ_x noise is given by

$$\begin{aligned} \rho(t) = & P \left[f_1 W(\theta_1, \theta_2) \rho(t-1) W(\theta_1, \theta_2)^\dagger f_1^\dagger \right] \\ & + (1 - P) W(\theta_1, \theta_2) \rho(t-1) W(\theta_1, \theta_2)^\dagger, \quad (18) \end{aligned}$$

where $\rho(0) = |\Psi_{\text{in}}\rangle\langle\Psi_{\text{in}}|$, $W(\theta_1, \theta_2)$ is same as Eq. (13), $f_1 \equiv \sigma_x \otimes \mathbb{I}$ and P is the magnitude of noise. No noise is described by $P = 0$ and due to the fact that symmetries are not effected by bit flip noise, the maximum noise corresponds to $P = 0.5$ ³⁵. In Fig. 10 we present the probability distribution and the corresponding value of

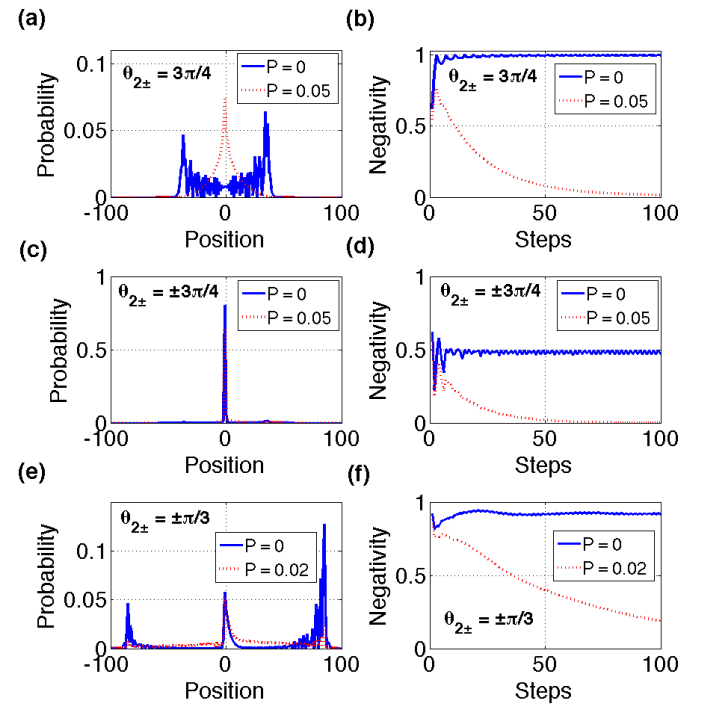


FIG. 10: Effect of σ_x noise on the two split-step DTQW for different configuration of $\theta_{2\pm}$ when $\theta_1 = -\pi/4$. (a), (c) and (e) show the probability distribution after 100 steps of walk in the absence and in the presence of noise. (b), (d) and (f) show the negativity as a function of the number of steps in absence and in presence of noise. The probability distributions show that the noise affects the diffusing part of the walk significantly but hardly influences the topologically localized part.

negativity for two split-step DTQW with different configuration of $\theta_{2\pm}$ for evolutions with and without noise. Applying noise to an evolution which in the absence of noise leads to a delocalized state (see Fig. 10(a), blue line), now leads to a state that is located around the origin. For a combination of $\theta_{2\pm}$ parameters resulting in a probability distribution with both, localized and a diffusive components (see Fig. 10(c) and (e)) the effect of noise results in a reduction of the probability for spreading in position space away from the origin, while the effect on the localized state is very small. This indicates the resistance of topologically localized states to noise when compared to distributions without localized states. In Figs. 10(b) and (d) the non-zero value of negativity shows the presence of the diffusive component in the probability distribution and with noise, this values decreases fast with increasing number of steps. In Fig. 10(e) we can see that even for noise as small as $P = 0.02$, the effect of noise on the delocalized probability distribution is very strong resulting in a the significant decrease of the probability away from the origin. However, the effect of noise on the localized

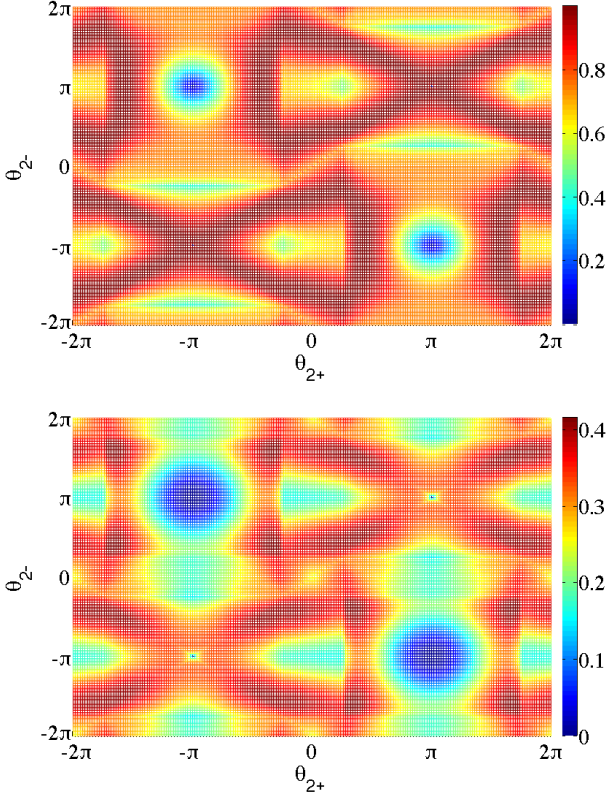


FIG. 11: Negativity as a function of θ_{2-} and θ_{2+} when $\theta_1 = -\pi/4$ for noise less and noisy two split-step DTQW. For (a) $P = 0.00$ and for (b) $P = 0.02$. Note the difference in the color scale.

part of the distribution is only very slight.

In Fig. 11 we present the negativity as function of θ_{2-} and θ_{2+} when $\theta_1 = -\pi/4$ for evolutions without and with σ_x noise of strength $P = 0.02$. One can see that the effect of the noise results in a decrease of the overall negativity, but remains essentially unchanged in the regions where strongly localized states appear. This indicates the robustness of the topologically localized state against σ_x noise.

However, topologically localized states in the two split-step DTQW are not robust to other forms of noise. In Fig. 12 we show the probability distributions for an evolution without (first row) and with noise (rest of the rows) after 100 (first column) and 200 (second column) steps. The σ_x noise is the same as given in Eq. (18) and the $\sigma_y = \begin{bmatrix} 0 & -i \\ i & 0 \end{bmatrix}$ and $\sigma_z = \begin{bmatrix} 1 & 0 \\ 0 & -1 \end{bmatrix}$ noises are obtained by replacing σ_x by σ_y and σ_z in the Eq. (18). The oper-

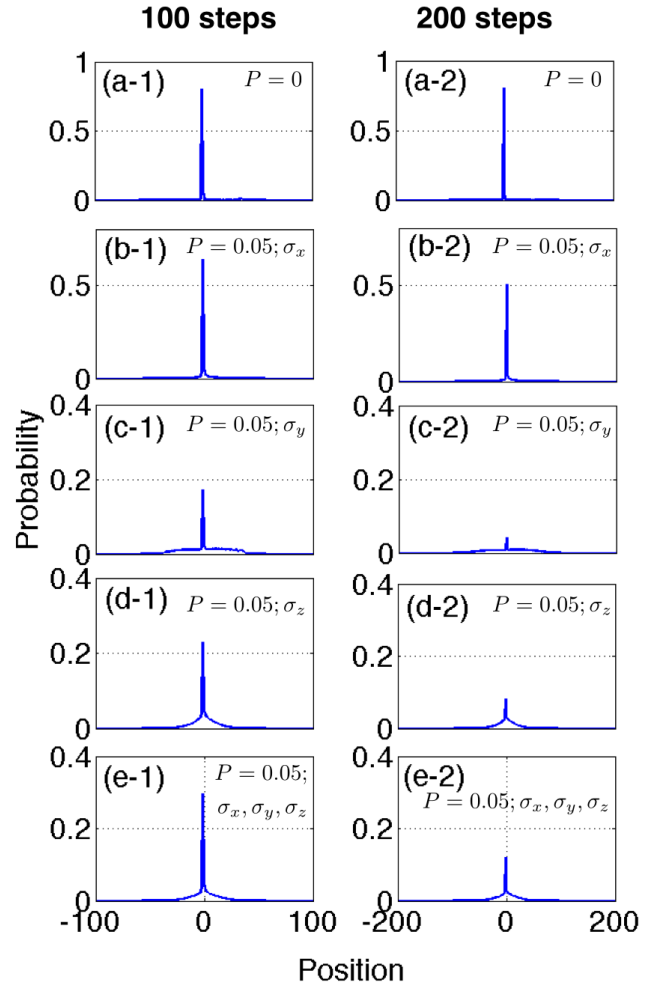


FIG. 12: Effect of noise on topologically localized states with $\theta_1 = -\pi/4$, $\theta_{2-} = -3\pi/4$ and $\theta_{2+} = 3\pi/4$. First and second column show the probability distribution after 100 step and 200 step of evolution, respectively. First row is the probability distribution for evolution without noise ((a-1), (a-2)), second row is for evolution with σ_x noise ((b-1), (b-2)), third row is for evolution with σ_y noise ((c-1), (c-2)), fourth row is for evolution with σ_z noise ((d-1), (d-2)) and the fifth row is for evolution with depolarizing noise ((e-1), (e-2)). For all the noisy evolution the noise level $P = 0.05$ and we can clearly see that localized state is robust against σ_x but for other forms of noise, we see a decrease in probability of localized state with time and small noise.

ation to describe depolarizing noise is given by

$$\begin{aligned} \rho(t) = & \frac{1}{3} \left[f_1 W(\theta_1, \theta_2) \rho(t-1) W(\theta_1, \theta_2)^\dagger f_1^\dagger + \right. \\ & f_2 W(\theta_1, \theta_2) \rho(t-1) W(\theta_1, \theta_2)^\dagger f_2^\dagger + \\ & f_3 W(\theta_1, \theta_2) \rho(t-1) W(\theta_1, \theta_2)^\dagger f_3^\dagger \left. \right] \\ & + (1-P) W(\theta_1, \theta_2) \rho(t-1) W(\theta_1, \theta_2)^\dagger. \quad (19) \end{aligned}$$

Comparing the probability distributions of the localized

states after evolution in the presence of these different kind of noises, one can clearly see that the topological states are robust only against σ_x noise and a significant decrease in localized probability at the interface is visible for all other forms of noise. From Eqs. (9) and (12) we can establish that the edge states at $\varepsilon = 0, \pi$ is the eigenstates of the chiral symmetry operator Γ and it is identical to $f_1(\sigma_x$ noise). The symmetry is preserved and therefore the edge state is not affected. However, for other forms of noise symmetry is not preserved and the localized state decays.

V. CONCLUSION

Engineering DTQWs with different combination of variable quantum coin and position shift operations allows to create a wide range of rich topological phases. Choosing parameters θ_i with different topological numbers to the left and right side of the interface of the position space, leads to topology induced localized states, sometimes accompanied by a diffusing component. Identifying combinations resulting strong localization with minimal or completely absent diffusing components is important for simulations of artificial TIs and in this work

we have shown that the negativity of a state can be used for such an identification. By exploring the negativity landscape as function of the quantum coin parameters we have linked the strength of the topologically localized states to the appearance of low values of the negativity.

These topology induced localized states are different from the localized states originating from disordered DTQWs, where the measure of entanglement is almost robust against disorder. This therefore allows to differentiate between topologically localized states and localized state due to spatial and dynamic disorder in 1D DTQW. Finally, we have demonstrated the robustness of topologically localized state against σ_x noise when compared to its effect of the diffusing component of the walk. We strongly believe that studies like this can lead to better engineering of the artificial materials to realize TIs.

Acknowledgments

This work was supported by the Okinawa Institute of Science and Technology Graduate University. H. O. was supported by Grant-in-Aid (Nos. 25800213 and 25390113) from the Japan Society for Promotion of Science.

^{*} Electronic address: c.madaiah@oist.jp

[†] Electronic address: hideaki.obuse@eng.hokudai.ac.jp

[‡] Electronic address: thomas.busch@oist.jp

¹ G. V. Riazanov, Sov. Phys., *The Feynman path integral for the Dirac equation*, Sov. Phys. JETP **6**, 1107-1113 (1958); R. Feynman, *Found. Phys.* **16**, 507-531 (1986); K. R. Parthasarathy, *Journal of Applied Probability*, **25**, 151-166 (1988).

² D. A. Meyer, *From quantum cellular automata to quantum lattice gases*, *J. Stat. Phys.* **85**, 551 (1996).

³ A. Ambainis, *Int. J. Quantum. Inform.* **01**, 507 (2003).

⁴ A. M. Childs, R. Cleve, E. Deotto, E. Farhi, S. Gutmann, and D. A. Spielman, *Exponential algorithmic speedup by quantum walk*, Proc. 35th ACM Symposium on Theory of Computing, pages 59-68 (2003).

⁵ M. Szegedy, *Quantum speed-up of Markov chain based algorithms*, Foundations of Computer Science, 2004. Proceedings. 45th Annual IEEE Symposium on, pages 32-41 (2004).

⁶ S. Aaronson and A. Ambainis, *Quantum search of spatial regions*, Theory of Computing, 1(4):47-79 (2005).

⁷ F. Magniez and A. Nayak, *Quantum complexity of testing group commutativity*, *Algorithmica*, 48(3):221-232 (2007).

⁸ A. Ambainis. *Quantum walk algorithm for element distinctness*, *SIAM Journal on Computing*, 37(1):210-239 (2007).

⁹ F. Magniez, A. Nayak, P. Richter, and M. Santha, *On the hitting times of quantum versus random walks*, *Algorithmica*, 63(1):91-116 (2012).

¹⁰ A.M. Childs, *Universal computation by quantum walk*, *Phys. Rev. Lett.* **102**, 180501 (2009).

¹¹ N. B. Lovett, S. Cooper, M. Everitt, M. Trevers, and V. Kendon, *Universal quantum computation using the discrete-time quantum walk*, *Phys. Rev. A* **81**, 042330 (2010).

¹² T. Oka, N. Konno, R. Arita, and H. Aoki, *Breakdown of an Electric-Field Driven System: A Mapping to a Quantum Walk*, *Phys. Rev. Lett.* **94**, 100602 (2005).

¹³ Engel, G. S. et al., *Evidence for wavelike energy transfer through quantum coherence in photosynthetic systems*, *Nature* **446**, 782-786 (2007).

¹⁴ Mohseni, M., Rebentrost, P., Lloyd, S. & Aspuru-Guzik, A. *Environment-assisted quantum walks in photosynthetic energy transfer*, *J. Chem. Phys.* **129**, 174106 (2008).

¹⁵ Plenio, M. B. & Huelga, S. F. *Dephasing-assisted transport: quantum networks and biomolecules*, *New J. Phys.* **10**, 113019 (2008).

¹⁶ F. D. Strauch, *Relativistic effects and rigorous limits for discrete- and continuous-time quantum walks*, *J. Math. Phys.* **48**, 082102 (2007).

¹⁷ C. M. Chandrashekar, S. Banerjee, & R. Srikanth, *Relationship between quantum walks and relativistic quantum mechanics*, *Phys. Rev. A* **81**, 062340 (2010).

¹⁸ Giuseppe, D. M., Debbasch, F. & Brachet, M. E., *Quantum walks as massless Dirac Fermion in curved space-time*, *Phys. Rev. A* **88**, 042301 (2013).

¹⁹ C. M. Chandrashekar, *Two-component Dirac-like Hamiltonian for generating quantum walk on one-, two- and three-dimensional lattices*, *Scientific Reports* **3**, 2829 (2013).

²⁰ M. Z. Hasan and C. L. Kane, *Colloquium: Topological insulators*, *Rev. Mod. Phys.* **82**, 3045 (2010).

²¹ X.-L. Qi and S.-C. Zhang, *Topological insulators and superconductors*, *Rev. Mod. Phys.* **83**, 1057 (2011).

²² J. E. Moore, *The birth of topological insulators*, *Nature*

(London) **464**, 194-1998 (2010).

²³ T. Kitagawa, M. S. Rudner, E. Berg, and E. Demler, *Exploring topological phases with quantum walks*, Phys. Rev. A **82**, 033429 (2010).

²⁴ H. Obuse and N. Kawakami, *Topological phases and delocalization of quantum walks in random environments*, Phys. Rev. B **84**, 195139 (2011).

²⁵ T. Kitagawa, M. A. Broome, A. Fedrizzi, M. S. Rudner, E. Berg, I. Kassal, A. Aspuru-Guzik, E. Demler, and A. G. White, *Observation of topologically protected bound states in photonic quantum walks*, Nature Communications **3**, 882 (2012).

²⁶ J. K. Asbóth, *Symmetries, topological phases, and bound states in the one-dimensional quantum walk*, Phys. Rev. B **86**, 195414 (2012).

²⁷ J. K. Asbóth and H. Obuse, *Bulk-boundary correspondence for chiral symmetric quantum walks* Phys. Rev. A **88**, 121406(R) (2013).

²⁸ B. Tarasinski, J. K. Asbóth, and J. P. Dahlhaus, *Scattering theory of topological phases in discrete-time quantum walks*, Phys. Rev. A **89**, 042327 (2014).

²⁹ J. Du et al., Phys. Rev. A **67**, 042316 (2003); C. A. Ryan et al., Phys. Rev. A **72**, 062317 (2005); B. Do et al., J. Opt. Soc. Am. B **22**, 499 (2005); H. B. Perets et al., Phys. Rev. Lett. **100**, 170506 (2008); H. Schmitz et al., Phys. Rev. Lett. **103**, 090504 (2009); F. Zahringer et al., Phys. Rev. Lett. **104**, 100503 (2010); K. Karski et al., Science **325**, 174 (2009); A. Schreiber et al., Phys. Rev. Lett., **104**, 050502 (2010); M. A. Broome et al., Phys. Rev. Lett. **104**, 153602 (2010); A. Peruzzo et al., Science **329**, 1500 (2010); L. Sansoni et al., Phys. Rev. Lett. **108**, 010502 (2012); A. Schreiber K. N. Cassemiro, V. Potocek, A. Gábris, I. Jex, and Ch. Silberhorn, *Decoherence and Disorder in Quantum Walks: From Ballistic Spread to Localization*, Phys. Rev. Lett. **106**, 180403 (2011); A. Crespi et al., *Anderson localization of entangled photons in an integrated quantum walk*, Nat. Phot. **7**, 323 (2013); J. D. A. Meinecke et al., *Coherent Time Evolution and Boundary Conditions of Two-Photon Quantum Walks*, Phys. Rev. A **88**, 012308 (2013).

³⁰ A. P. Schnyder, S. Ryu, A. Furusaki, and A. W. W. Ludwig, *Classification of topological insulators and superconductors in three spatial dimensions* Phys. Rev. B, **78**, 195125 (2008).

³¹ C. M. Chandrashekar, arXiv:1212.5984 (2012).

³² R. Vieira, E. P. M. Amorim, and G. Rigolin, Phys. Rev. Lett. **111**, 180503 (2013).

³³ O. Maloyer and V. Kendon, *Decoherence versus entanglement in coined quantum walks*, New J. Phys. **9**, 87 (2007).

³⁴ S. K. Goyal and C. M. Chandrashekar, *Spatial entanglement using a quantum walk on a many-body system*, J. Phys. A: Math. Theor. **43**, 235303 (2010).

³⁵ C. M. Chandrashekar, R. Srikanth, and S. Banerjee, *Symmetries and noise in quantum walk*, Phys. Rev. A, **76**, 022316 (2007).